Preparation, Characterization, and Photoactivity of Polycrystalline Nanostructured TiO_2 Catalysts

Maurizio Addamo,[†] Vincenzo Augugliaro,[†] Agatino Di Paola,[†] Elisa García-López,[†] Vittorio Loddo,[†] Giuseppe Marcì,[†] Raffaele Molinari,[‡,§] Leonardo Palmisano,*[,†] and Mario Schiavello[†]

Dipartimento di Ingegneria Chimica dei Processi e dei Materiali, Università di Palermo, Viale delle Scienze, 90128 Palermo, Italy, and Dipartimento di Ingegneria Chimica e dei Materiali, Università della Calabria, Via P. Bucci, 87030 Rende (CS), Italy.

Received: December 8, 2003

Various preparations of nanostructured TiO_2 starting from Ti(iso-OC_3H_7)$_4$ or $TiCl_4$ are reported. The samples were characterized by X-ray diffractometry, specific surface area and porosity determinations, scanning and transmission electron microscopy, and diffuse reflectance spectroscopy. 4-Nitrophenol photodegradation in aqueous medium was employed as a probe reaction to test the photoactivity of the catalysts. The photoactivity of some samples derived from Ti(iso-OC_3H_7)$_4$ was found comparable with that of commercial powders. Calcination after the hydrolysis process was necessary to achieve crystallization of the particles before using them as photocatalysts for the reaction studied. The samples deriving from $TiCl_4$ were the most photoactive among the home-prepared catalysts, and neither filtration nor calcination was needed to obtain a highly photoactive anatase phase.

Introduction

Heterogeneous photocatalysis has been found effective for the achievement of the photooxidation of many organic pollutants present in liquid effluents[1−4] or in air as VOCs.[5,6] This method offers some advantages compared to the traditional ones because it is not selective; the reactions usually occur at room temperature and atmospheric pressure, and UV radiations of low intensity are needed.

TiO_2 is the most used photocatalyst, due to its (photo)stability and low cost.[7] The preparation methods are reported to influence significantly morphological, structural, surface physicochemical, and electronic properties that are related to the extent of photoactivity.[8,9] Unfortunately, near-UV photons (band gaps equal to 3.2 and 3.0 eV for anatase and rutile phases, respectively) are needed for the excitation of TiO_2. This drawback can be overcome by using not stoichiometric or doped TiO_2 because a bathochromic shift in the light absorption is generally observed in those cases. Nevertheless this phenomenon does not give rise always to an enhancement of the photoactivity of the material.[10−13]

Recently, many studies have been reported on the preparation and characterization of various nanostructured semiconductors because it has been found that the nanoparticles exhibit special photochemical characteristics.[14−19] In particular, the band gap of the nanoparticles increases with the decrease of the size and other important properties such as optical and physical absorption and luminescence emission undergo drastic changes.

TiO_2 nanoparticles have been recently employed in photocatalysis for photodegradation of noxious species in aqueous medium,[20−24] although the existence of stable nanoparticles is known to be not easy, due to their tendency to agglomerate. Even if in most cases the samples used did not consist of discrete nanoparticles but only of nanostructured particles, this kind of photocatalysts is reported to show a high photoactivity compared with that of many commercial samples.[23−28] On the other hand, the presence of very small particles cannot be excluded when the photoreactivity experiments are carried out in mixed liquid−solid systems. The use of submicrometric particles is possible today by means of membrane photoreactors.[29]

In this paper different TiO_2 samples, consisting of nanostructured particles, were prepared by taking into account the up-to-date literature[27−31] but changing the starting precursors, Ti(iso-OC_3H_7)$_4$ or $TiCl_4$, and/or modifying some operative parameters such as molar ratio of the reagents, heating and calcination temperatures, and times.

Bulk and surface characterizations of the powders were carried out by means of X-ray diffractometry (XRD), determination of the BET specific surface areas, porosity measurements, scanning electron microscopy (SEM), transmission electron microscopy (TEM), and diffuse reflectance spectroscopy (DRS) techniques. 4-Nitrophenol photodegradation was employed as a probe reaction in order to test the photoactivity of the home-prepared samples compared with that of some commercial samples.

Experimental Section

Catalysts Preparation. Titanium isopropoxide, titanium tetrachloride, ethanol, and 2-propanol were obtained from Carlo Erba. All chemicals were used as received. The commercial TiO_2 samples were Degussa P25, Merck and Tioxide.

The preparation methods for various nanostructured TiO_2 samples were the following:

Preparation 1. Titanium hydroxide was prepared by hydrolysis of titanium isopropoxide carried out at room temperature

* Corresponding author. Tel: +39-091-6567246. Fax: +39-091-6567280. E-mail: palmisan@dicpm.unipa.it.
† Università di Palermo.
‡ Università della Calabria.
§ Tel: +39-0984-492090. Fax: +39-0984-492058. E-mail: r.molinari@unical.it.

10.1021/jp0312924 CCC: $27.50 © 2004 American Chemical Society
Published on Web 02/11/2004

for 1 h in a mixture of water and 2-propanol (molar ratios Ti/2-propanol/H_2O equal to 1:22:5; volume (mL) ratios 10:60:3):

$$Ti(iso\text{-}OC_3H_7)_4 + 4H_2O \rightarrow Ti(OH)_4 + 4C_3H_7OH$$

The precipitate was then filtered, and different portions were successively calcined for 24 h at 573, 673, or 773 K. The following code was used for the samples: P1-TiO_2(i-Pr, 573, 673, or 773) where i-Pr indicates 2-propanol and 573, 673, or 773 the calcination temperature in Kelvin.

Preparation 2. A highly dispersed stable colloidal suspension of titanium hydroxide was prepared by hydrolysis of titanium isopropoxide carried out at 333 K for 5 h in a mixture of ethanol, strong acid, and water. The strong acids used were HCl (37%) or HNO_3 (65%), (molar ratios Ti/ethanol/H^+/H_2O equal to 1:20:0.5:200; volume (mL) ratios 10:40:2:130 using HCl or 10:40:1:130 using HNO_3). The suspension was dried at 323 K and the obtained solid was washed with water. Successively different fractions were calcined at 573, 673, or 773 K for 24 h. The following codes were used for the samples: P2-TiO_2(Cl, 573, 673, or 773) and P2-TiO_2(N, 573, 673, or 773), where Cl and N indicate HCl and HNO_3, respectively.

Preparation 3. Titanium hydroxide was prepared by hydrolysis of titanium isopropoxide in a mixture of ethanol and water (molar ratios Ti/ethanol/H_2O equal to 1:5:200; volume (mL) ratios 10:11:130) carried out at 333 K for 5 h. The suspension was then dried at 323 K, and successively different fractions were calcined for 24 h at 573, 673, or 773 K. The following code was used for the samples: P3-TiO_2(Et, 573, 673, or 773) where Et indicates ethanol.

Preparation 4. A sol was prepared by hydrolysis of titanium tetrachloride at room temperature for 24 h (molar ratios Ti/water equal to 1:60; volume (mL) ratios 10:100). The resulting clear solution was boiled for ca. 3 h in order to form a solid and to eliminate at the same time most of chloride ions as $HCl_{(g)}$. In some cases, the boiling times were 1, 12, or 24 h. The code used for these samples was P4-TiO_2(ex $TiCl_4$, h) where h indicates the boiling time. The dispersions containing very small particles were directly employed for the photoreactivity experiments. Some dispersions were tested after 7, 30, or 90 days of aging. The characterization of all samples was carried out on the solids obtained by drying the dispersion at ca. 323 K.

Sample Characterization. *X-ray Diffraction.* XRD patterns of the powders were recorded at room temperature by a Philips powder diffractometer using the Cu Kα radiation and a 2θ scan rate of 2°/min. X-ray diffraction was used for crystal phase identification and estimation of the crystallite size of each phase present. The percentage of rutile in the samples was determined from the respective integrated XRD peak intensities using the following equation:[32] $\chi = (1 + 0.8I_A/I_R)^{-1}$, where χ is the weight fraction of rutile in the powder, and I_A and I_R are the X-ray intensities obtained from the areas of the peaks relative to the 101 and 110 reflections of anatase and rutile, respectively, which are the most intense reflections in the diffractograms.

The crystallite size was estimated from the Scherrer formula: $\Phi = K\lambda/(\beta \cos \theta)$ where Φ is the crystallite size, λ is the wavelength of the X-ray radiation (0.154 nm), K is usually taken as 0.89, β is the peak width at half-maximum height after subtraction of the equipment broadening, $2\theta = 25.3°$ and $2\theta = 27.4°$ for TiO_2 (anatase) and TiO_2 (rutile), respectively.

Specific Surface Area and Porosity. The specific surface areas were determined in a Flow Sorb 2300 apparatus (Micromeritics) by using the single-point BET method. Porosity was monitored from the nitrogen adsorption−desorption isotherms obtained at the liquid nitrogen temperature on samples degassed for 2 h at 523 K prior to the measurement, using a Sorptomatic 1900 Carlo Erba Instrument.

XPS Analysis. The X-ray photoelectron spectroscopy analyses were performed by means of a VG Microtech ESCA 3000 Multilab, equipped with a dual Mg/Al anode. The working pressure was around 1×10^{-6} Pa. The samples were analyzed as pellets after being ground in a mortar.

Scanning Electron Microscopy. SEM observations were obtained using a model Philips XL30 ESEM microscope, operating at 25 kV on specimens upon which a thin layer of gold had been evaporated. For some samples a drop of suspension on the stab was directly dried at room temperature or sprayed and dried after dilution (1:10 v/v).

Transmission Electron Microscopy. The particle size of the powders has been determined by using a JEOL JEM 12−20 transmission electron microscope (TEM) and the micrographs were recorded at 120 kV. The samples were prepared by dispersing the powders in water and depositing a drop of suspension onto a thin Formavar film supported on a Cu grid.

Diffuse Reflectance Spectroscopy. Visible−ultraviolet spectra were obtained by diffuse reflectance spectroscopy by using a Shimadzu UV-2401 PC instrument. $BaSO_4$ was the reference sample and the spectra were recorded in the range 200−800 nm.

Photoreactivity Experiments. A Pyrex batch photoreactor of cylindrical shape containing 0.5 liters of aqueous suspension was used. The photoreactor was provided with ports in its upper section for the inlet and outlet of gases, for sampling, and for pH and temperature measurements. A 125 W medium-pressure Hg lamp (Helios Italquartz, Italy) was immersed within the photoreactor and the photon flux emitted by the lamp was $\Phi_i = 13.5$ mW cm^{-2}. It was measured by using a radiometer "UVX Digital" leaned against the external wall of the photoreactor containing only pure water. O_2 was continuously bubbled into the suspensions for ca. 0.5 h before switching on the lamp and throughout the occurrence of the photoreactivity experiments. The temperature inside the reactor was ca. 300 K. The quantitative determination of 4-nitrophenol was performed by measuring its absorption at 315 nm with a spectrophotometer Shimadzu UV-2401 PC. Nonpurgeable organic carbon (NPOC) determinations were performed by using a Shimadzu TOC analyzer 5000-A.

Samples Obtained by Preparations 1−3. The amount of catalyst was always 1.0 g L^{-1}, and the initial 4-nitrophenol (BDH) concentration was ca. 20 mg L^{-1}. The initial pH of the suspension was adjusted to 2 by addition of HNO_3 (Carlo Erba RPE), and a milky dispersion was obtained. The photoreactivity runs lasted 6.0 h including the first half hour during which the lamp was switched off. Samples of 5 mL volume were withdrawn from the suspensions every 5, 30, or 60 min, and the catalyst was separated from the solution by filtration through 0.10 μm Teflon membranes (Whatman).

Samples Obtained by Preparation 4. To obtain the amount of catalyst (ca. 1 g L^{-1}) employed for the photoreactivity runs, the necessary volume of suspension was determined by the weight of the solid obtained drying directly 10 mL of suspension. An alternative procedure consisted in weighing the precipitate separated after adjustment of the pH of the suspension to ca. 7 with 1 M NaOH . In both cases similar values were found.

Results and Discussion

Characterization. Titanium isopropoxide and titanium tetrachloride have been chosen as precursors for the preparation of

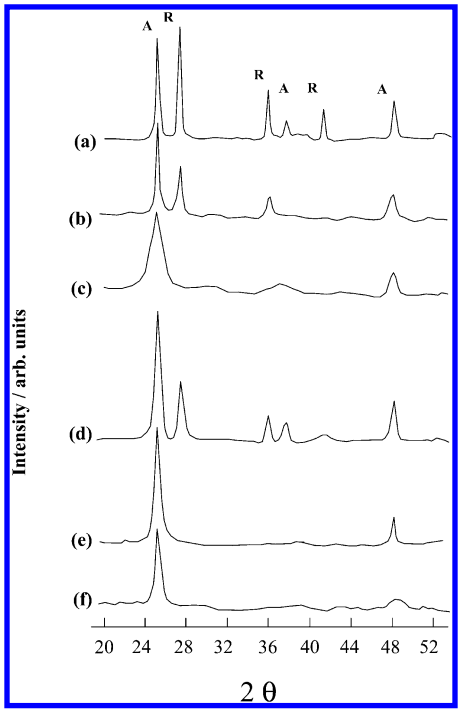

Figure 1. XRD diffractograms of P2-TiO_2(Cl, 773) (a); P2-TiO_2(Cl, 673) (b); P2-TiO_2(Cl, 573) (c);- P2-TiO_2(N, 773) (d); P2-TiO_2(N, 673) (e); P2-TiO_2(N, 573) (f). A = anatase, R = rutile.

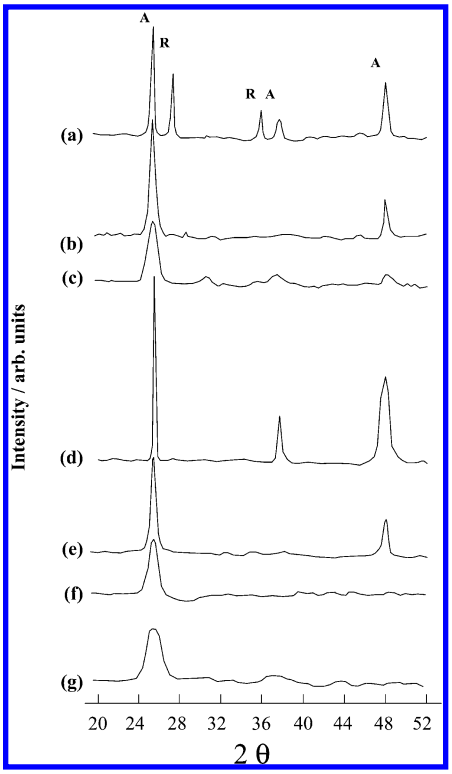

Figure 2. XRD diffractograms of P3-TiO_2(Et, 773) (a); P3-TiO_2(Et, 673) (b); P3-TiO_2(Et, 573) (c); P1-TiO_2(i-Pr, 773) (d); P1-TiO_2(i-Pr, 673) (e); P1-TiO_2(i-Pr, 573) (f); P4-TiO_2(ex $TiCl_4$, 3) (g). A = anatase, R = rutile.

nanostructured TiO_2 catalysts since both Ti(iso-$OC_3H_7)_4$[33−40] and $TiCl_4$[41−47] are largely used to prepare nanophase TiO_2 particles. The properties of the sol−gel derived catalysts depend on the preparation conditions including the kind of solvent, solution preparation sequence, aging temperature, boiling time, and calcination temperature.

Figures 1 and 2 show the X-ray diffraction patterns of some selected samples. The diffractograms indicate only the presence of a badly crystallized anatase phase for all of the samples obtained by preparations 1−3 and calcined at 573 K. The samples calcined at 673 K consist of a better crystallized anatase phase with the exception of P2-TiO_2(Cl, 673) for which a mixture of anatase and rutile phases was found. The last result indicates a positive influence of the chloride ions on the crystallization process of the rutile phase. This is in agreement with the findings of Jung and Park[39] who observed rutile peaks over 673 K for TiO_2 particles obtained from titanium isopropoxide in the presence of HCl. It is worth noting that also the hydrothermal treatment of amorphous TiO_2 suspensions prepared from $TiCl_4$ leads to the formation of a small amount of rutile when HCl is used as a cooperative catalyst for the peptization process.[41,42] Zhang and Gao[48] found that HCl peptization accelerates the anatase-to-rutile phase transformation of the TiO_2 nanoparticles prepared by hydrolysis of metatitanic acid and reduces the phase transformation temperature.

The samples calcined at 773 K, with the exception of P1-TiO_2(i-Pr, 773), consist of a mixture of anatase and rutile phases in different amounts, depending on the preparation. The presence of Cl^- seems to favor the formation of rutile even at this temperature.

The kind of solvent used influences the crystallization behavior, porosity, and microstructure of the TiO_2 powders prepared through hydrolysis and condensation of titanium alkoxides in aqueous media.[37,49] The effect probably arises from the different abilities of the various solvents to allow condensation and aggregation of the particles. An important role is also played by the molar ratio water/precursor. Kim et al.[31] found that the phase rutile begins to appear only at 873 K in the powders obtained by hydrolysis of titanium isopropoxide in a water/ethanol mixture. According to Terabe et al.,[34] the presence of residual unhydrolyzed alkyls prevents the crystallization of the powders. This effect decreases with increasing the amount of H_2O or HCl addition. The presence of rutile in the sample P3-TiO_2(Et,773) calcined at 773 K is probably due to the initial large water concentration.

Starting by $TiCl_4$, preparation 4 allows us to obtain a photoactive (see Photoreactivity Experiments) anatase phase, although badly crystallized, in experimental conditions milder than those used in hydrothermal processes carried out at higher pressures in closed vessels.[23−28, 40−42]

The phases present in the various samples and their relative amounts are reported in Table 1 together with the diameter of crystallites determined by the Sherrer equation indicating that all the samples tested are nanostructured. The microcrystallites sizes range from 5 to 40 nm. The size of the particles, as expected, increases by increasing the calcination temperature. P3-TiO_2(Et, 573) and P2-TiO_2(Cl, 773) consist of the smallest and the biggest particles, respectively.

The size of the particles formed in 2-propanol is slightly higher than that of the particles obtained in the presence of ethanol. This effect could be ascribed to the different dielectric constants of the two solvents. By increasing the molecular weight of the alcohol, the dielectric constant of the solvent decreases, lowering the electrostatic barrier against the aggregation of the primary particles.[50] As found by Vorkapic and Matsoukas,[38] the result is decreased stability, enhanced rate of reaggregation, and formation of larger particles.

Nitrogen adsorption−desorption isotherms were used to ascertain the porosity of the catalysts. The inset of Figure 3 displays a typical example of the isotherms obtained with the various samples. The curves were similar, irrespective of the

TABLE 1: Bulk and Physicochemical Properties of the Samples

sample	phase[a]	Φ[b] (nm)	SSA[c] ($m^2\ g^{-1}$)	$r_0 \times 10^9$ [d] (mol $L^{-1}\ s^{-1}$)
P1-TiO_2(i-Pr, 573)	A (badly cryst.)	8	124	10
P1-TiO_2(i-Pr, 673)	A (100%)	15	98	19
P1-TiO_2(i-Pr, 773)	A(100%)	30	79	20
P2-TiO_2(N, 573)	A (badly cryst.)	10	104	negligible
P2-TiO_2(N, 673)	A (100%)	11	27	negligible
P2-TiO_2(N, 773)	A(50%), R(50%)	15[A], 23[R]	3	negligible
P2-TiO_2(Cl, 573)	A (badly cryst.)	7	126	negligible
P2-TiO_2(Cl, 673)	A(56%), R(44%)	20[A], 26[R]	32	negligible
P2-TiO_2(Cl, 773)	A(22%), R(78%)	40[A], 33[R]	14	negligible
P3-TiO_2(Et, 573)	A (badly cryst.)	5	150	13
P3-TiO_2(Et, 673)	A (100%)	7	101	20
P3-TiO_2(Et, 773)	A(60%), R(40%)	15[A], 33[R]	49	22
P4-TiO_2(ex$TiCl_4$, 1)	A (badly cryst.)	8	105	10
P4-TiO_2(ex$TiCl_4$, 3)	A (badly cryst.)	8	115	35
P4-TiO_2(ex$TiCl_4$, 12)	A (badly cryst.)	8	110	16
P4-TiO_2(ex$TiCl_4$, 24)	A (badly cryst.)	8	100	10
Degussa P25	A(80%), R(20%)	25[A], 33[R]	50	50
Tioxide	A (100%)		7	40
Merck	A (100%)	60	10	20

[a] A = anatase, R = rutile. [b] Φ = diameter of crystallites calculated by the Scherrer equation. [c] SSA = BET specific surface area. [d] r_0 = initial reaction rate for 4-nitrophenol degradation.

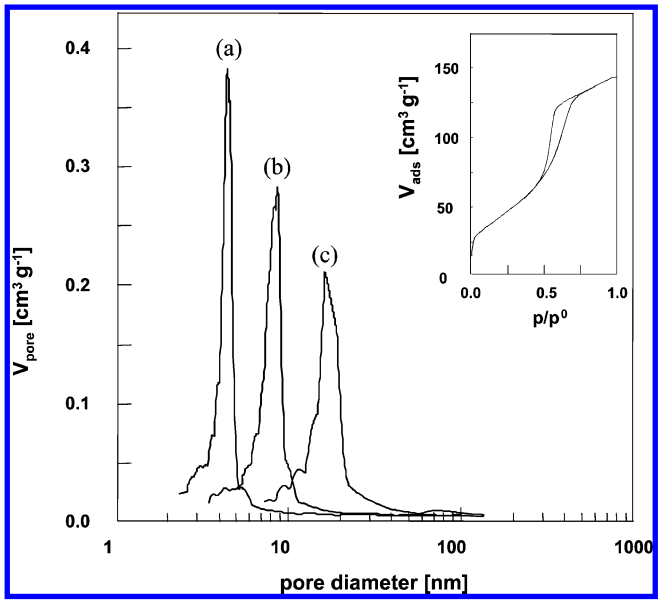

Figure 3. Pore size distribution for the samples obtained according to preparation 1: P3-TiO_2(Et, 573) (a); P3-TiO_2(Et, 673) (b); P3-TiO_2(Et, 773) (c). Inset: N_2 adsorption−desorption isotherm of P3-TiO_2(Et, 573).

preparation method. According to the IUPAC classification,[51] the isotherms were of type IV and exhibited hysteresis loops of type H2. Thus all the samples were mesoporous and the pores were networked.[51,52] The mesoporous structure was retained after calcination at 673 and 773 K, revealing that the close-packed agglomeration remained although the surface areas of the samples decreased (see below) due to the grain growth.

The pore size distribution was calculated using the Dollimore-Heal method.[53] Figure 3 shows the pore size distribution of the samples obtained from ethanol after calcination at different temperatures. The distribution profiles of all the curves were almost the same, but the maximum of the pore size distribution shifted toward larger pore diameters with increasing the calcination temperature. In particular, the maximum pore size increased from ca. 7 nm at 573 K to 14 nm at 773 K. The decreasing pore volume is ascribable to the collapse of the network (smallest pores) during the calcination.

The samples obtained from propanol and calcined at the same temperatures revealed pore sizes slightly smaller than those exhibited by the powders prepared from ethanol. The porosity of the samples derived from $TiCl_4$ was not determined since outgassing at 523 K for 2 h could cause irreversible changes in the texture of these catalysts.

The BET specific surface areas (SSA) of the samples (see Table 1) decrease by increasing the calcination temperature. The SSA values of P4-TiO_2(ex $TiCl_4$, h), not subjected to calcination, are similar to those of the other samples derived from preparations 1−3 calcined at 573 K and appear quite independent of the boiling time.

The decrease of SSA for the samples obtained by means of preparation 2 (in the presence of HCl or HNO_3) was generally more significant with respect to the corresponding samples prepared in the absence of acids. The collapse of the porous network during the calcination treatment does not seem attributable to a detrimental role played by residual traces of inorganic species since XPS analysis (with the exception of P2-TiO_2(Cl, 573) containing ca. 1.3 at. % of Cl) did not reveal appreciable amounts of Cl^- or NO_3^- on the surface of these samples.

Selected SEM micrographs of P1-TiO_2(i-Pr, 573), P3-TiO_2(Et, 673), P3-TiO_2(Et, 773), and P4-TiO_2(ex $TiCl_4$, 3) are shown in Figure 4. The samples present irregular shapes and consist of aggregates of particles whose sizes appear generally bigger than those calculated by the Sherrer equation, due probably to the difficulty to obtain good micrographs at a high resolution. All the powders have small primary particles and larger secondary particles. The close-packed agglomeration of the particles causes probably the formation of mesoporous samples.

The micrographs reveal a remarkable effect of the calcination temperature on the size of the aggregates of crystallites. Indeed the biggest particles (ca. 90−170 nm) are present in the samples calcined at 773 K (Figure 4c), while the smallest ones (ca. 40−50 nm) are exhibited by the samples calcined at 573 K (Figure 4a) and by the sample P4-TiO_2(ex $TiCl_4$, 3) (Figure 4d) that was not subjected to calcination. In particular the particles of the last sample consist of aggregates whose size is more uniform than that of samples derived from the other preparations.

In Figure 5, SEM micrographs of P4-TiO_2(ex $TiCl_4$, 24) and P4-TiO_2(ex $TiCl_4$, 3) with 90 days of aging are reported. It can be noted that the primary particles (between 100 and 300 nm) and the secondary ones (bigger than 2 μm) of the samples obtained after 24 h of boiling or after 90 days of aging appear

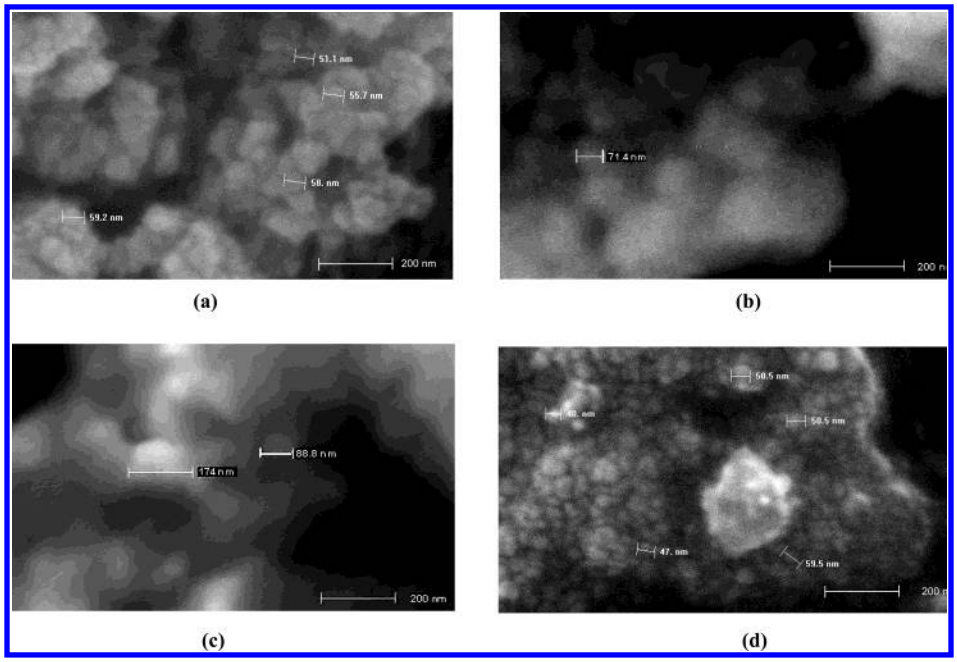

Figure 4. Selected SEM micrographs of P1-TiO_2(i-Pr, 573) (a); P3-TiO_2(Et, 673) (b); P3-TiO_2(Et, 773) (c); P4-TiO_2(ex $TiCl_4$, 3) (d). Magnification: ×100,000.

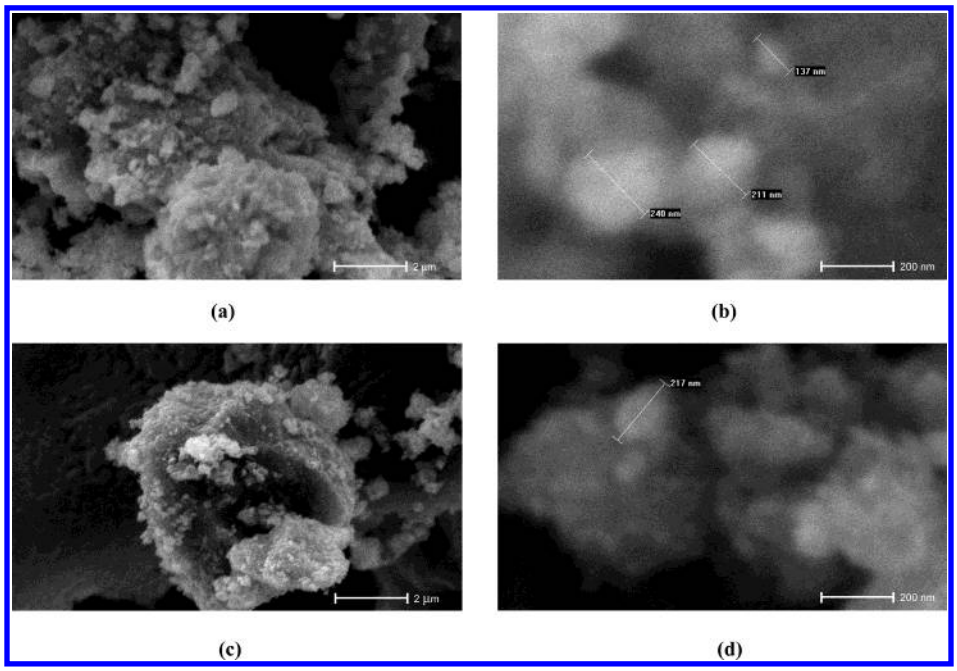

Figure 5. Selected SEM micrographs of P4-TiO_2(ex $TiCl_4$, 24) (a) and (b); P4-TiO_2(ex $TiCl_4$, 3) after 90 days of aging (c) and (d). Magnification: (a) and (c) ×10,000; (b) and (d) ×100,000.

to be larger than those observed in the micrograph of the sample obtained after 3 h of boiling, without aging (see Figure 4d).

TEM micrographs of P3-TiO_2(Et, 573), P3-TiO_2(Et, 673), and P3-TiO_2(Et, 773) samples are shown in Figure 6. These micrographs indicate that the size of the primary particles of the samples is quite uniform and in accord with the figures obtained by means of the Scherrer equation.

Figure 7 shows the diffuse reflectance spectra of some samples. Spectra (a), (b), and (d) of well crystallized samples indicate that the band-gap energy increases by increasing the amount of anatase. The spectrum of the P4-TiO_2(ex $TiCl_4$, 3) sample is similar to that of Degussa P25, although a straightforward comparison cannot be done, due to its bad crystallinity.

Photoreactivity Experiments. The apparent kinetics of disappearance of 4-nitrophenol was followed by determining the concentration of the substrate at various time intervals. Figure 8 shows the results of 4-nitrophenol oxidation in the presence of commercial TiO_2 powders and of representative samples obtained according to different preparations. The values of the initial reaction rate (r_0) are reported in Table 1.

The calcination temperature seems a key factor strongly influencing the photoactivity and, in particular, the highest values of r_0 were obtained with the samples calcined at 673 and 773 K. The photoactivity of the calcined samples increases with increasing the crystallinity of the particles although the surface area is reduced. Calcination is used to improve the crystallinity of the powders since the existence of amorphous contents has generally detrimental effects on the photocatalytic properties of TiO_2 nanoparticles,[28] due to the recombination of

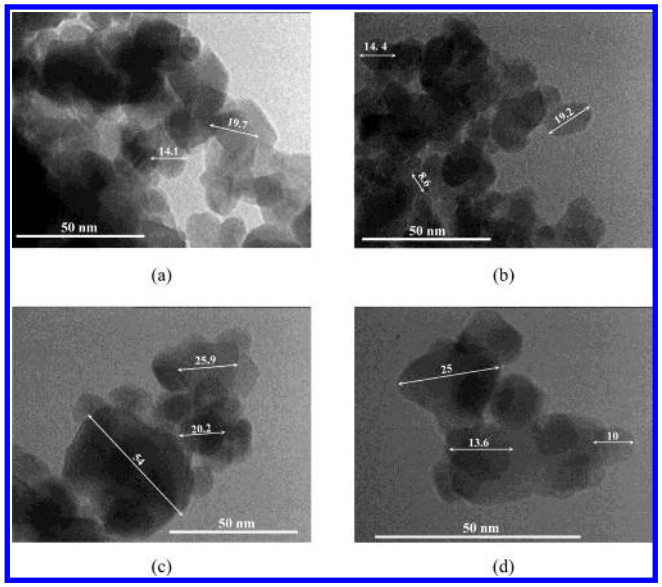

Figure 6. Selected TEM micrographs of P3-TiO_2(Et, 573) (a); P3-TiO_2(Et, 673) (b); P3-TiO_2(Et, 773) (c). Magnification: ×250,000. P3-TiO_2(Et, 573) (d). Magnification: ×400,000.

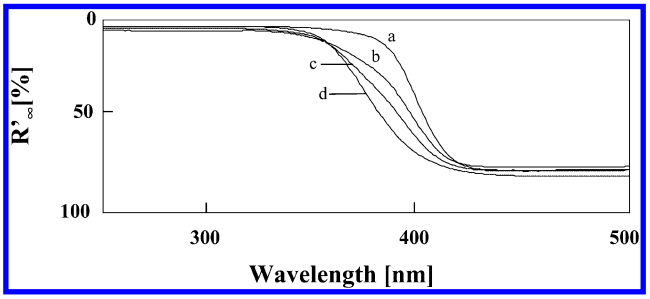

Figure 7. Diffuse reflectance spectra of selected samples: P2-TiO_2(Cl, 773) (a); P3-TiO_2(Et, 773) (b); P4-TiO_2 (ex $TiCl_4$, 3) (c); Degussa P25 (d).

photoexcited electrons and holes at defects located on the surface and in the bulk of the particles.[54]

As shown in Table 1, the photoactivity of the rutile/anatase mixed phase P3-TiO_2(Et, 773) was higher than that of the pure anatase samples. This is in agreement with the results of Bickley et al.[55] and Fotou and Pratsinis[56] reporting that TiO_2 photocatalysts containing some rutile are more active than the samples containing only anatase. Moreover, mixed rutile/anatase nanoparticles prepared from titanium isopropoxide[42] or from $TiCl_4$[25] have been found to be more active than pure anatase.

Both P2 sets did not show appreciable photoactivity independent of the calcination temperature, indicating that the presence of HNO_3 or HCl is detrimental. On the contrary, P1-TiO_2(i-Pr, 673), P1-TiO_2(i-Pr, 773), P3-TiO_2(Et, 673), P3-TiO_2(Et, 773), and P4-TiO_2(ex $TiCl_4$, 3) revealed a photocatalytic activity quite comparable with that of the three commercial samples.

P4-TiO_2(ex $TiCl_4$, 3) appears to be the most promising catalyst from an application point of view among the various home-prepared samples because neither separation and washing of the solid nor its calcination were needed to obtain a highly active photocatalyst. It is worth reminding indeed that a photoactive anatase phase was obtained only by means of treatment in very mild experimental conditions. Several runs were carried out by using the suspension containing the photocatalyst, that was stable at pH = 2, simply by adding the model pollutant and afterward transferring the dispersion in the batch photoreactor. The photoactivity of P4-TiO_2(ex $TiCl_4$, 3)

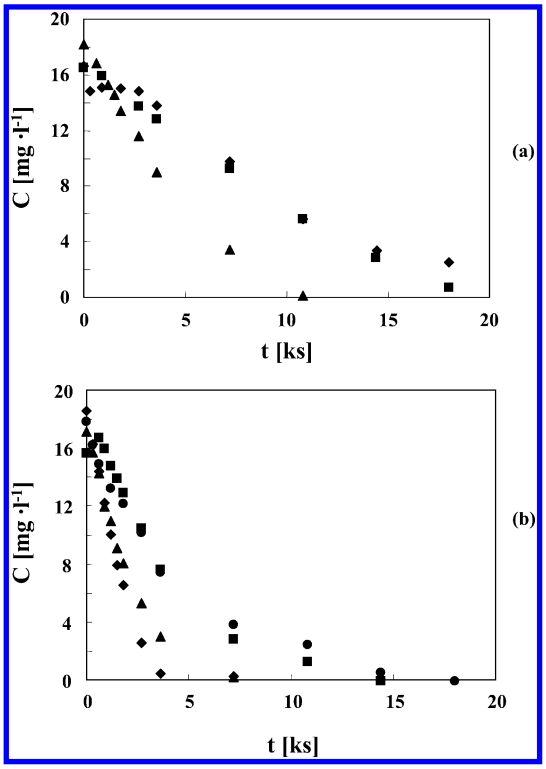

Figure 8. 4-Nitrophenol concentration versus irradiation time: (a) P3-TiO_2(Et, 573) (◆), P3-TiO_2 (Et, 673) (■), P3-TiO_2(Et, 773) (▲); (b) Degussa P25 (◆), Merck (■), Tioxide (▲), P4-TiO_2(ex $TiCl_4$, 3) (●).

($r_0 = 35 \times 10^{-9}$ mol L^{-1} s^{-1}) was tested also without any adjustment of pH value (in this case the pH was ca. 1). No substantial difference of the initial observed reaction rate was found, indicating that the presence of Na^+ deriving from NaOH used to adjust the pH was not detrimental.

Some tests were carried out by using P4-TiO_2(ex $TiCl_4$, 12) and P4-TiO_2(ex $TiCl_4$, 24) samples. The final pH values of the suspensions were ca. 1.5 and 2, respectively, and for both cases sedimentation of the catalyst particles was observed by stopping mixing due, probably, to an increase of their size. The activity of these photocatalysts decreased by increasing the boiling time ($r_0 = 16 \times 10^{-9}$ mol L^{-1} s^{-1} for 12 h boiling and $r_0 = 10 \times 10^{-9}$ mol L^{-1} s^{-1} for 24 h boiling). The comparison with the photoactivity observed by using the sample boiled for 1 h ($r_0 = 10 \times 10^{-9}$ mol L^{-1} s^{-1}) suggests an optimal boiling time between 2 and 4 h.

P4-TiO_2(ex $TiCl_4$, 3) was also tested at pH = 5 and pH = 10. For both pH values an aggregation of particles was observed and the following lower values of initial reaction rates were obtained: $r_0 = 10 \times 10^{-9}$ mol L^{-1} s^{-1} for pH = 5 and $r_0 = 9.6 \times 10^{-9}$ mol L^{-1} s^{-1} for pH = 10 ($r_0 = 35 \times 10^{-9}$ mol L^{-1} s^{-1} for pH = 2).

Figure 9 shows selected experiments carried out by using the dispersion of P4-TiO_2(ex $TiCl_4$, 3) after 7, 30, or 90 days of aging. No significant differences were found between fresh and one-week-aged catalysts, but a decreasing photoactivity was observed by increasing the times of aging (30 and 90 days). The decrease of photoactivity observed in both cases (prolonged boiling or aging) is probably related to the growth of the particles (see Figure 5), although the influence of other physicochemical factors cannot be excluded.

Figure 10 shows the decrease of the nonpurgeable organic carbon (NPOC) with the irradiation time for some representative runs. All the samples appear to be effective to mineralize completely 4-nitrophenol although after different times. The

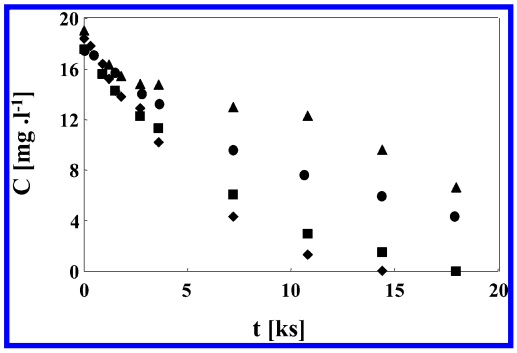

Figure 9. 4-Nitrophenol concentration versus irradiation time for P4-TiO_2(ex $TiCl_4$, 3): fresh (◆), 7 days aged (■), 30 days aged (●), and 90 days aged (▲).

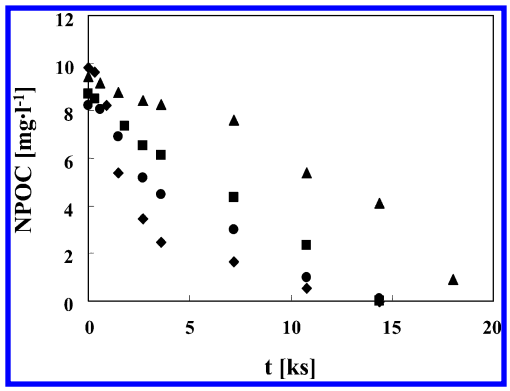

Figure 10. Nonpurgeable organic carbon versus irradiation time: Degussa P25 (◆), P3-TiO_2(Et, 773) (■), P1-TiO_2(i-Pr, 573) (▲), P4TiO_2(ex $TiCl_4$, 3) (●).

mineralization rate in the initial reaction steps was generally low, probably due to the accumulation of organic intermediates. It can be noticed that by using the P4-TiO_2(ex $TiCl_4$, 3) sample a complete mineralization was achieved after a time comparable with that of Degussa P25 (ca. 4 h). The use of this nanostructured catalyst in a hybrid membrane photocatalytic reactor could be useful because of its very easy "in situ" preparation. Studies are in progress on the behavior of this submicrometric catalyst in hybrid photoreactors.

Conclusions

Nanostructured TiO_2 catalysts having various particle sizes and phase composition were prepared by different preparations. The differences of photoreactivity exhibited by the various samples depended on the preparation procedures, the calcination temperature, and the different values of the specific surface areas. The samples obtained by hydrolysis of titanium isopropoxide in mixtures of water and alcohol and in the absence of acid (preparation 1 and 3) showed an increasing rate of the photodegradation reaction of 4-nitrophenol as the calcination temperature increased. This is attributable to the effect of the presence of a well-crystallized anatase phase that plays a more important role than that of the particle size.

The results indicate that the presence of HCl or HNO_3 has detrimental effects on the photocatalytic properties since the samples prepared by mixtures ethanol-strong acid−water revealed negligible photoactivitites even though the phases and the size of the particles were similar to those of the samples obtained in neutral solutions.

The photocatalytic activity of some powders approaches that of commercial TiO_2 catalysts. In particular, the results of several tests show that the samples derived from $TiCl_4$ exhibit the best results, and the technique presented here seems an economical and fast way for the preparation of a highly active photocatalyst.

Acknowledgment. The authors thank the Ministero dell'Istruzione, dell'Università e della Ricerca, MIUR, Rome (Progetto L. 488 of Interuniversity National Consortium "Chemistry for the Environment", INCA) for the financial support of this work and Dr. V. Marcianò for the assistance in recording the TEM micrographs. We are indebted to Dr. N. Liotta and Dr. A. M. Venezia for the porosity and XPS measurements.

References and Notes

(1) *Photocatalysis and Environment. Trends and Applications*; Schiavello, M., Ed.; Kluwer Academic Publishers: Dordrecht, 1988.
(2) *Photocatalysis. Fundamentals and Applications*; Pelizzetti, E., Serpone, N., Eds.; John Wiley & Sons: New York, 1989.
(3) Linsebigler, A. L.; Lu, G.; Yates, J. T., Jr. *Chem. Rev.* **1995**, *95*, 735.
(4) Herrmann, J. M. *Helv. Chim. Acta* **2001**, *84*, 2731.
(5) Peral, J.; Domenech, X.; Ollis, D. F. *J. Chem. Technol. Biotechnol.* **1997**, *70*, 117.
(6) Augugliaro, V.; Coluccia, S.; Loddo, V.; Marchese, L.; Martra, G.; Palmisano, L.; Schiavello, M. *Appl. Catal. B: Environ.* **1999**, *20*, 15.
(7) Fujishima, A.; Hashimoto, K.; Watanabe, T. *TiO_2 Photocatalysis: Fundamentals and Applications*; Bkc: Tokyo, 1999.
(8) Sclafani, A.; Palmisano, L.; Schiavello, M. *J. Phys. Chem.* **1990**, *94*, 829.
(9) Kominami, H.; Kohno, M.; Matsunaga, Y.; Kera, Y. *J. Am. Ceram. Soc.* **2001**, *84*, 1178.
(10) Venezia, A. M.; Palmisano, L.; Schiavello, M.; Martín, C.; Martín, I.; Rives, V. *J. Catal.* **1994**, *147*, 115.
(11) Litter, M. I. *Appl. Catal B: Environ.* **1999**, *23*, 89.
(12) Yamashita, H.; Harada, M.; Misaka, J.; Takeuchi, M.; Ichihashi, Y.; Goto, F.; Ishida, M.; Sasaki, T.; Anpo, M. *J. Synchroton Rad.* **2001**, *8*, 569.
(13) Di Paola, A.; Marcì, G.; Palmisano, L.; Schiavello, M.; Uosaki, K.; Ikeda, S.; Othani, B. *J. Phys. Chem. B* **2002**, *106*, 637.
(14) Nozik, A. J. In *Photocatalytic Purification and Treatment of Water and Air*; Ollis, D. F., Al-Ekabi, H., Eds.; Elsevier: Amsterdam, 1993; p 39.
(15) Hagfeldt, A.; Grätzel, M. *Chem. Rev.* **1995**, *95*, 49.
(16) Anpo, M. *Catal. Surveys from Japan* **1997**, *1*, 169.
(17) Beydoun, D.; Amal, R.; Low, G.; McEvoy, S. *J. Nanoparticle Res.* **1999**, *1*, 439.
(18) Miyake, M.; Torimoto, T.; Sakata, T.; Mori, H.; Yoneyama, H. *Langmuir* **1999**, *15*, 1503.
(19) Torimoto, T.; Kontani, H.; Shibutani, Y.; Kuwabata, S.; Sakata, T.; Mori, H.; Yoneyama, H. *J. Phys. Chem. B* **2001**, *105*, 6838.
(20) Pal, B.; Sharon, M. *J. Mol. Catal. A: Chem.* **2000**, *160*, 453.
(21) Bahnemann, D. W.; Kholuiskaya, S. N.; Dillert, R.; Kulak, A. I.; Kokorin, A. I. *Appl. Catal. B: Environ.* **2002**, *36*, 161.
(22) Skubal, L. R.; Meshkov, N. K.; Rajh, T.; Thurnauer, M. *J. Photochem. Photobiol. A: Chem.* **2002**, *148*, 393.
(23) Zhang, Z.; Wang, C. C.; Zakaria, R.; Ying, J. Y. *J. Phys. Chem. B* **1998**, *102*, 10871.
(24) Kominami, H.; Kato, J.-i.; Murakami, S.-Y.; Kera, Y.; Inoue, M.; Inui, T.; Ohtani, B. *J. Mol. Catal. A: Chem.* **1999**, *144*, 165.
(25) Zhang, Q. H.; Gao, L.; Guo, J. *Appl. Catal. B: Environ.* **2000**, *26*, 207.
(26) Hashimoto, K.; Wasada, K.; Toukai, N.; Kominami, H.; Kera, Y. *J. Photochem. Photobiol. A: Chem.* **2000**, *136*, 103.
(27) Maira, A. J.; Yeung, K. L.; Soria, J.; Coronado, J. M.; Belver, C.; Lee, C. Y.; Augugliaro, V. *Appl. Catal. B: Environ.* **2001**, *29*, 327.
(28) Kominami, H.; Kumamoto, H.; Kera, Y.; Ohtani, B. *Appl. Catal. B: Environ.* **2001**, *30*, 329.
(29) Molinari, R.; Palmisano, L.; Drioli, E.; Schiavello, M. *J. Membr. Sci.* **2002**, *206*, 399.
(30) Gao, L.; Zhang, Q. *Scripta. Mater.* **2001**, *44*, 1195.
(31) Kim, J.; Song, K. C.; Pratsinis, S. E. *J. Nanoparticle Res.* **2000**, *2*, 419.
(32) Spurr, R. A.; Myers, H. *Anal. Chem.* **1957**, *29*, 760.
(33) Dagan, G.; Tomkiewicz, M. *J. Phys. Chem.* **1993**, *97*, 12651.
(34) Terabe, K.; Kato, K.; Miyazaki, H.; Yamaguchi, S.; Imai, A.; Iguchi, Y. *J. Mater. Sci.* **1994**, *29*, 1617.
(35) Choi, W.; Termin, A.; Hoffmann, M. R. *J. Phys. Chem.* **1994**, *98*, 13669.
(36) Khalil, K. M. S.; Zaki, M. I. *Powder Technol.* **1997**, *92*, 233.
(37) Wu, K.-T.; Spencer, H. G.; *J. Non-Cryst. Solids* **1998**, *226*, 249.
(38) Vorkapic, D.; Matsoukas, T. J. *Am. Ceram. Soc.* **1998**, *81*, 2815.

(39) Jung, K. Y.; Park, S. B. *J. Photochem. Photobiol. A: Chem.* **1999**, *127*, 117.
(40) Burnside, S. D.; Shklover, V.; Barbé, C.; Comte, P.; Arendse, F.; Brooks, K.; Grätzel, M. *Chem. Mater.* **1998**, *10*, 2419.
(41) Yin, H.; Wada, Y.; Kitamura, T.; Kambe, S.; Murasawa, S.; Mori, H.; Sakata, T.; Yanagida, S. *J. Mater. Chem.*, **2001**, *11*, 1694.
(42) Yanagisawa, K.; Ovenstone, J. *J. Phys. Chem. B* **1999**, *103*, 7781.
(43) Anpo, M.; Shima, T.; Kodama, S.; Kubokawa, Y. *J. Phys. Chem.* **1987**, *91*, 4305.
(44) Kormann, C.; Bahnemann, D. W.; Hoffmann, M. R. *J. Phys. Chem.* **1988**, *92*, 5196.
(45) Pelizzetti, E.; Minero, C.; Borgarello, E.; Tinucci, L.; Serpone, N. *Langmuir* **1993**, *9*, 2995.
(46) Zhang, Q. H.; Gao, L.; Guo, J. K. *Nanostruct. Mater*. **1999**, *11*, 1293.
(47) Eremenko, B. V.; Bezuglaya, T. N.; Savitskaya, A. N.; Malysheva, M. L.; Kozlov, I. S.; Bogodist, L. G. *Colloid J.* **2001**, *63*, 173.
(48) Zhang, R.; Gao, L. *Mater. Res. Bull.* **2001**, *36*, 1957.
(49) Hu, L.; Yoko, T.; Kozuka, H.; Sakka, S. *Thin Solid Films* **1992**, *219*, 18.
(50) Moon, Y. T.; Park, H. K.; Kim, D. K.; Kim, C. H. *J. Am. Ceram. Soc*. **1995**, *78*, 2690.
(51) Sing, K. S. W.; Everett, D. H.; Haul, R. A. W.; Moscou, L.; Pierotti, R. A.; Rouquérol, J.; Siemienieniewska, T. *Pure Appl. Chem*. **1985**, *57*, 603.
(52) Gregg, S. J. In *Adsorption at the Gas−Solid and Liquid−Solid Interfaces*; Roquerol, J., King, K. S. W., Eds.; Elsevier: Amsterdam, 1982; pp 153−164.
(53) Dollimore, D.; Heal, G. R. *J. Appl. Chem*. **1964**, *14*, 109.
(54) Ohtani, B.; Ogawa, Y.; Nishimoto, S.-i. *J. Phys. Chem. B* **1197**, *101*, 3746.
(55) Bickley, R. I.; González-Carreño, T.; Lees, J. S.; Palmisano, L.; Tilley, R. J. D. *J. Solid State Chem.* **1991**, *92*, 178.
(56) Fotou, G. P.; Pratsinis, S. *Chem. Eng. Commun*. **1996**, *151*, 251.